GENERATION OF HIMAWARI-8 AMVs USING THE FUTURE MTG AMV PROCESSOR

Manuel Carranza [1], Régis Borde [2], Masahiro Hayashi [3]

[1] GMV Aerospace and Defence S.A. at EUMETSAT, Eumetsat Allee 1, D-64295 Darmstadt, Germany
[2] EUMETSAT, Eumetsat Allee 1, D-64295 Darmstadt, Germany
[3] Meteorological Satellite Center, Japan Meteorological Agency, 3-235 Nakakiyoto, Kiyose, Tokyo 204-0012, Japan

Abstract

The Meteosat Third Generation (MTG) programme is intended to provide meteorological data from the geostationary orbit as a continuation of the Meteosat Second Generation (MSG) services at least until the late 2030s. The first MTG satellite is scheduled for a launch around 2019. The programme consists of a twin satellite concept, based on three-axis stabilised platforms: four imaging satellites (MTG-I) and two sounding satellites (MTG-S). Images from the Flexible Combined Imager (FCI) instrument on board the MTG-I satellites will be used to derive Atmospheric Motion Vectors (AMVs) in a wide range of frequencies, from visible to infrared.

The nested tracking algorithm developed at NOAA has been recently tested at EUMETSAT using MSG data in order to assess its potential benefits for MTG, and the results have been compared to those of CLA and OCA.

In preparation for the upcoming launches, the MSG AMV processor has been adapted to Himawari-8 as a first step towards adapting it to MTG. Himawari-8 was launched in October 2014 and provides operational services since July 2015. The Advanced Himawari Imager (AHI) instrument on board Himawari-8 is a 16 channel multispectral imager, and has similar spectral and spatial characteristics to the aforementioned MTG-I FCI instrument. In this paper, preliminary results of the MTG AMV processor using Himawari-8 data are presented.

MSG NESTED TRACKING RESULTS

The nested tracking (NT) algorithm, described in Daniels et al. (2012), is being tested at EUMETSAT, as shown in Carranza et al. (2014). A series of tests have been recently conducted, where the nested tracking algorithm in various configurations is compared with the current MSG algorithm (using both CLA and OCA height assignment methods). A five-day period, 14th to 18th April 2016, was selected. Only channel 10.8 µm has been considered so far, but future tests will involve other channels as well.

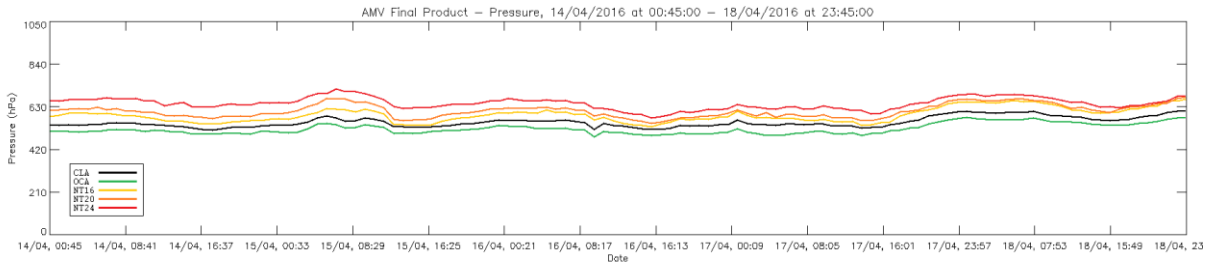

Figure 1: **Time series of average AMV pressure for CLA (black), OCA (green), NT 16x16 (light orange), NT 20x20 (dark orange), and NT 24x24 (red).**

Figure 1 shows the time series of average AMV pressure for the different configurations: CLA (black),

OCA (green), NT using a target box size of 16x16 pixels (light orange), NT using 20x20 pixels (dark orange), and NT using 24x24 pixels (red). The average pressure is smallest for OCA (521 hPa), then CLA (554 hPa), and then nested tracking, with consistently larger values for larger target box sizes (589 hPa, 608 hPa and 645 hPa, respectively).

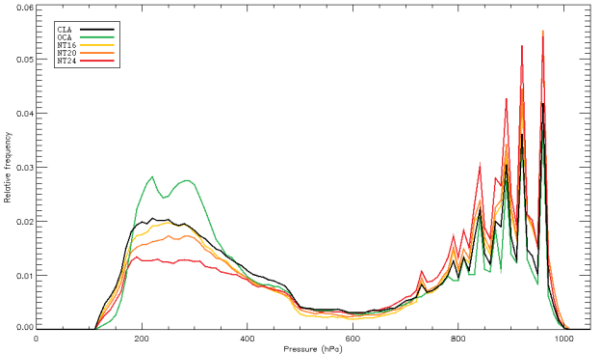

Figure 2: **Average AMV pressure histograms for CLA (black), OCA (green), NT 16x16 (light orange), NT 20x20 (dark orange), and NT 24x24 (red).**

Figure 2 shows the average AMV pressure histograms for the different configurations. There is a clear redistribution of pressures from high levels to low levels when moving from OCA to CLA to NT (in accordance with the values observed in Figure 1).

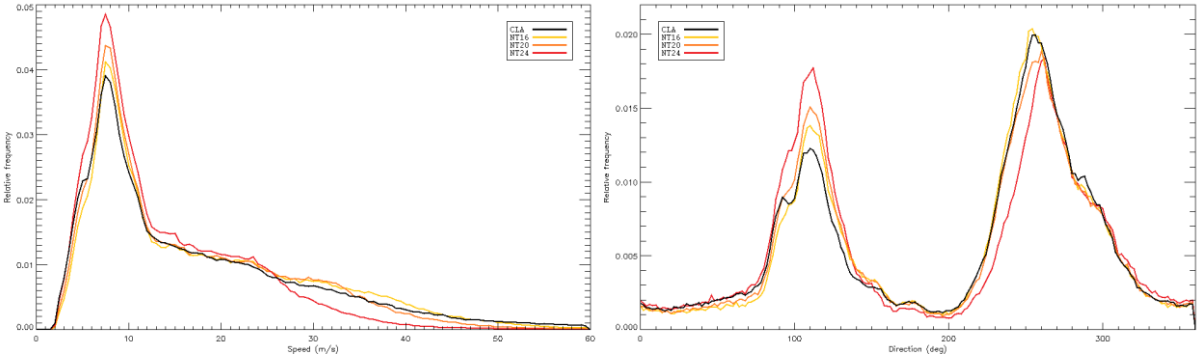

Figure 3: **Average AMV speed (left) and direction (right) histograms for CLA / OCA (black), NT 16x16 (light orange), NT 20x20 (dark orange), and NT 24x24 (red).**

Figure 3 shows the average AMV speed (left) and direction (right) histograms for the different configurations. The values for CLA and OCA are the same, because the tracking is identical in both cases. The histograms are very similar in all cases, with nested tracking yielding a larger amount of slow winds with larger target box sizes. This is in agreement with the general observation that the smaller the target box, the faster the AMVs, as shown in García-Pereda et al. (2014).

AMV speed statistics

Region	ALL	HGH	MID	LOW
GLO	**0.49**	0.72	1.08	-0.12
NH	1.07	1.73	0.21	0.36
TR	2.04	2.62	3.67	0.68
SH	-2.45	-4.50	-0.50	-1.38

Region	ALL	HGH	MID	LOW
GLO	**0.45**	0.41	0.48	0.42
NH	0.43	0.37	0.54	0.58
TR	0.49	0.47	0.64	0.35
SH	0.39	0.36	0.35	0.41

Table 1: **Average AMV speed bias (left) and speed NRMS (right) using CLA (GLO = global, NH = northern hemisphere, TR = tropics, SH = southern hemisphere). Speed bias values are in m/s.**

Region	ALL	HGH	MID	LOW
GLO	0.16	0.51	-0.36	-0.30
NH	0.55	1.73	-2.31	-0.36
TR	1.90	2.40	2.58	0.65
SH	-3.11	-4.98	-1.64	-1.58

Region	ALL	HGH	MID	LOW
GLO	0.44	0.40	0.51	0.41
NH	0.42	0.35	0.62	0.56
TR	0.47	0.46	0.57	0.33
SH	0.40	0.37	0.36	0.40

Table 2: **Average AMV speed bias (left) and speed NRMS (right) using OCA (GLO = global, NH = northern hemisphere, TR = tropics, SH = southern hemisphere). Speed bias values are in m/s.**

Table 1 and Table 2 show the average AMV speed bias and speed NRMS using CLA and OCA, respectively, as a function of the geographical area and the pressure level.

Region	NT 16x16				NT 20x20				NT 24x24			
	ALL	HGH	MID	LOW	ALL	HGH	MID	LOW	ALL	HGH	MID	LOW
GLO	0.86	1.42	1.89	-0.11	0.32	0.67	0.91	-0.20	-0.51	-0.76	-0.32	-0.36
NH	1.94	2.86	1.55	0.44	0.80	1.53	-0.01	0.20	-0.88	-0.84	-2.17	-0.15
TR	2.51	3.40	5.26	0.79	2.06	2.88	4.38	0.70	1.11	1.26	3.27	0.61
SH	-2.12	-4.13	0.11	-1.32	-2.46	-4.76	-0.71	-1.50	-2.75	-5.40	-1.78	-1.78

Table 3: **Average AMV speed bias using nested tracking (GLO = global, NH = northern hemisphere, TR = tropics, SH = southern hemisphere). All values are in m/s.**

Region	NT 16x16				NT 20x20				NT 24x24			
	ALL	HGH	MID	LOW	ALL	HGH	MID	LOW	ALL	HGH	MID	LOW
GLO	0.42	0.39	0.45	0.38	0.43	0.41	0.45	0.38	0.47	0.46	0.49	0.38
NH	0.40	0.34	0.51	0.50	0.42	0.35	0.53	0.50	0.50	0.41	0.62	0.50
TR	0.47	0.45	0.64	0.31	0.48	0.46	0.63	0.31	0.48	0.49	0.60	0.31
SH	0.38	0.35	0.32	0.37	0.39	0.38	0.33	0.38	0.42	0.43	0.36	0.38

Table 4: **Average AMV speed NRMS using nested tracking (GLO = global, NH = northern hemisphere, TR = tropics, SH = southern hemisphere).**

Table 3 and Table 4 show the average AMV speed bias and speed NRMS, respectively, for the nested tracking algorithm in the various configurations specified.

According to the tables above, the statistics are very similar for CLA and NT, especially (NT 20x20), and they are slightly better for OCA in some areas. However, the speed bias shows significant differences, not only between CLA or OCA and NT, but also among the various NT configurations themselves. Indeed, it can be noted that for nested tracking the larger the target box, the smaller the speed bias. Moreover, the average AMV speed bias is positive for CLA, OCA, NT 16x16 and NT 20x20, but it is negative for NT 24x24. This can be noted particularly in the northern hemisphere, but also in the tropics and the southern hemisphere. So far it is unclear why this is the case, but it is believed that it might have something to do with the selection of cloud-edge pixels during the height assignment process. This will be further investigated in the near future.

Comparing CLA and OCA, the average AMV speed bias is in general smaller for OCA in absolute value. However OCA performs worse in the southern hemisphere and for mid-level AMVs in the northern hemisphere. In any case OCA seems to present a slight improvement in certain areas like

the tropics and at low levels. This has been confirmed by analyses done at ECMWF.

The values for the speed NRMS are very similar in all cases, with slightly smaller values for nested tracking. Particularly, the values are almost identical for CLA and OCA.

Computing times

Algorithm	1 hour	1 day
CLA / OCA	5.00 min	2.0 hours
NT 16x16	11.25 min	4.5 hours
NT 20x20	12.50 min	5.0 hours
NT 24x24	13.13 min	5.3 hours

Table 5: **Average computing times for one hour and one day of data.**

Table 5 shows the average computing times obtained with the different algorithms for the period considered. It can be noted that nested tracking takes at least twice as much time as the current CLA/OCA algorithm. Besides, the larger the target box, the longer it takes to run the algorithm. This is a drawback with respect to CLA/OCA, especially considering that the algorithm needs to run in a near-real-time system, where timeliness is a key element; but the impact of this is still to be assessed.

HIMAWARI-8 AMVs

Introduction to MTG

The Meteosat Third Generation (MTG) programme consists of a twin satellite concept, based on three-axis stabilised platforms (see Figure 4):

- four imaging satellites (MTG-I), to be operational for at least 20 years;
- two sounding satellites (MTG-S), to be operational for at least 15.5 years.

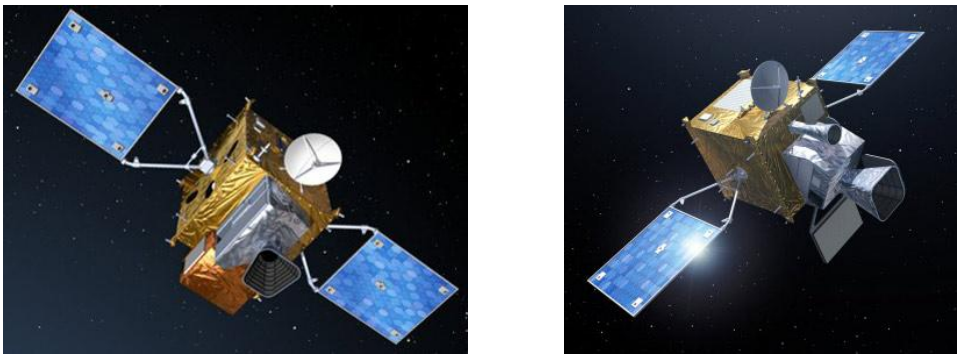

Figure 4: **MTG-I (left) and MTG-S (right) concepts (courtesy of ESA).**

The MTG-I satellite payload comprises the Flexible Combined Imager (FCI), the Lightning Imager (LI) and the Data Collection System (DCS), whereas the MTG-S satellite payload consists of the Infrared Sounder (IRS) and the Ultra-violet, Visible and Near-Infrared Sounder (UVN).

The FCI instrument on board the MTG-I satellites is a continuation of the very successful Spinning Enhanced Visible and Infrared Imager (SEVIRI) instrument on board the MSG satellites. FCI comprises a total of 16 spectral channels, with better spatial, temporal and radiometric resolution, compared to SEVIRI. Eight of the channels are in the solar spectral domain (0.4 µm to 2.1 µm), with 1 km resolution, whereas the other eight channels are in the thermal spectral domain (3.8 µm to 13.3

μm), with 2 km resolution.

The design allows for Full Disk Scan (FDS), with a basic repeat cycle of 10 minutes, and a European Regional Rapid Scan (RRS) which covers one-quarter of the full disk with a repeat cycle of 2.5 minutes.

Comparison of MTG's FCI and Himawari-8's AHI instruments

	MTG's FCI		
Channel	**Wavelength**	**Type**	**Spatial resol.**
1	0.44 μm	VIS	1 km
2	0.51 μm	VIS	1 km
3	0.64 μm	VIS	1 km
4	0.87 μm	VIS	1 km
5	0.91 μm	VIS	1 km
6	1.38 μm	NIR	1 km
7	1.61 μm	NIR	1 km
8	2.25 μm	NIR	1 km
9	3.80 μm	IR	2 km
10	6.30 μm	WV	2 km
11	7.35 μm	WV	2 km
12	8.70 μm	IR	2 km
13	9.66 μm	IR	2 km
14	10.50 μm	IR	2 km
15	12.30 μm	IR	2 km
16	13.30 μm	IR	2 km

	Himawari-8's AHI		
Channel	**Wavelength**	**Type**	**Spatial resol.**
1	0.47 μm	VIS	1 km
2	0.51 μm	VIS	1 km
3	0.64 μm	VIS	0.5 km
4	0.86 μm	VIS	1 km
5	1.61 μm	NIR	2 km
6	2.26 μm	NIR	2 km
7	3.88 μm	IR	2 km
8	6.24 μm	WV	2 km
9	6.94 μm	WV	2 km
10	7.35 μm	WV	2 km
11	8.59 μm	IR	2 km
12	9.64 μm	IR	2 km
13	10.41 μm	IR	2 km
14	11.24 μm	IR	2 km
15	12.38 μm	IR	2 km
16	13.28 μm	IR	2 km

Table 6: **MTG's FCI (left) vs Himawari-8's AHI (right) spectral channels.**

Table 6 shows the spectral channels of MTG's FCI instrument (on the right) and Himawari-8's AHI instrument (on the left). It can be appreciated that there is a direct correspondence for 14 of the 16 channels; only FCI's channels 5 and 6 are not available in AHI. The overall spectral and spatial characteristics of AHI are very similar to those of FCI, which makes Himawari-8's data a very valuable resource in testing the future MTG AMV processor.

The MTG AMV processor

The MTG AMV processor is largely based on the MSG AMV processor, with the following main characteristics:

- processing based on three images, instead of four;
- CCC method used for tracking;
- OCA used for height assignment, instead of CLA;
- computation of AMV height standard deviation and error;
- final AMV coordinates set to the position of the tracked feature;
- no intermediate product averaging; second intermediate component used as final product instead.

The MTG AMV processor has been adapted to be able to run using Himawari-8 data (images, cloud products, forecast, etc.). The algorithm has been developed so that it can be further adapted to other geostationary satellite (e.g. Meteosat First Generation) data easily. This will be done in the framework of the development of the MTG L2PF (Level 2 Processing Facility). It must be noted that the cloud product used by the MTG processor in this particular study is the one from JMA, not CLA/OCA.

First results

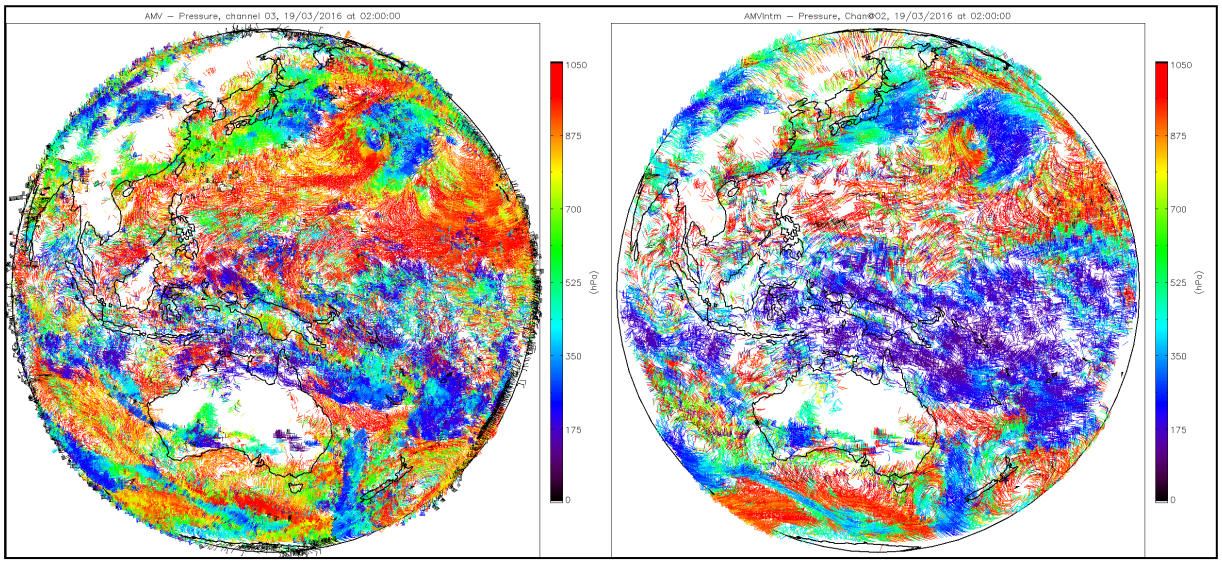

Figure 5: **Channel 0.64 µm AMVs, Himawari-8 (left) vs. MTG processor (right).**

Figure 5 shows the channel 0.64 µm (VIS) AMV fields on 19/03/2016 at 02:00 UTC for Himawari-8 (left) and the MTG processor (right). The results are very similar in both cases, especially concerning the tracking, but there are some obvious differences.

In general AMVs are located slightly higher in the atmosphere for the MTG processor than for Himawari-8 (i.e. there are more dark blue AMVs). There are also more very-low-level AMVs for MTG than for Himawari-8 (i.e. there are more deep red AMVs). This is caused by the application of an inversion correction algorithm within the MTG processor, which is not the case for the Himawari-8 processor. In any case, it must be noted that the pressure used in the calculation of the Himawari-8 AMVs is computed internally as part of the AMV process itself, whereas the pressure used by the MTG processor is directly obtained from the cloud-top pressure product provided by JMA; so the results are not expected to be 100% coincident. All in all, the general distribution of AMVs is very similar for both processors, which is a fair indication that the MTG processor works as intended.

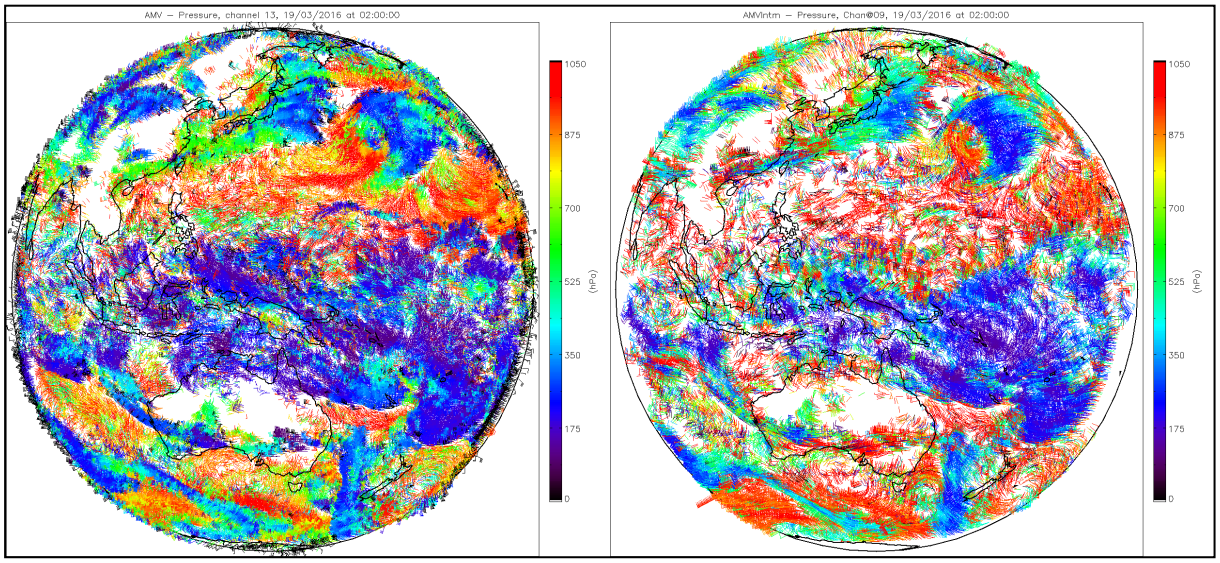

Figure 6: **Channel 10.41 µm AMVs, Himawari-8 (left) vs. MTG processor (right).**

Similarly, Figure 6 shows the channel 10.41 µm (IR) AMV fields on 19/03/2016 at 02:00 UTC. The results are again very similar in both cases, and the same basic conclusions can be extracted as for channel 0.64 µm.

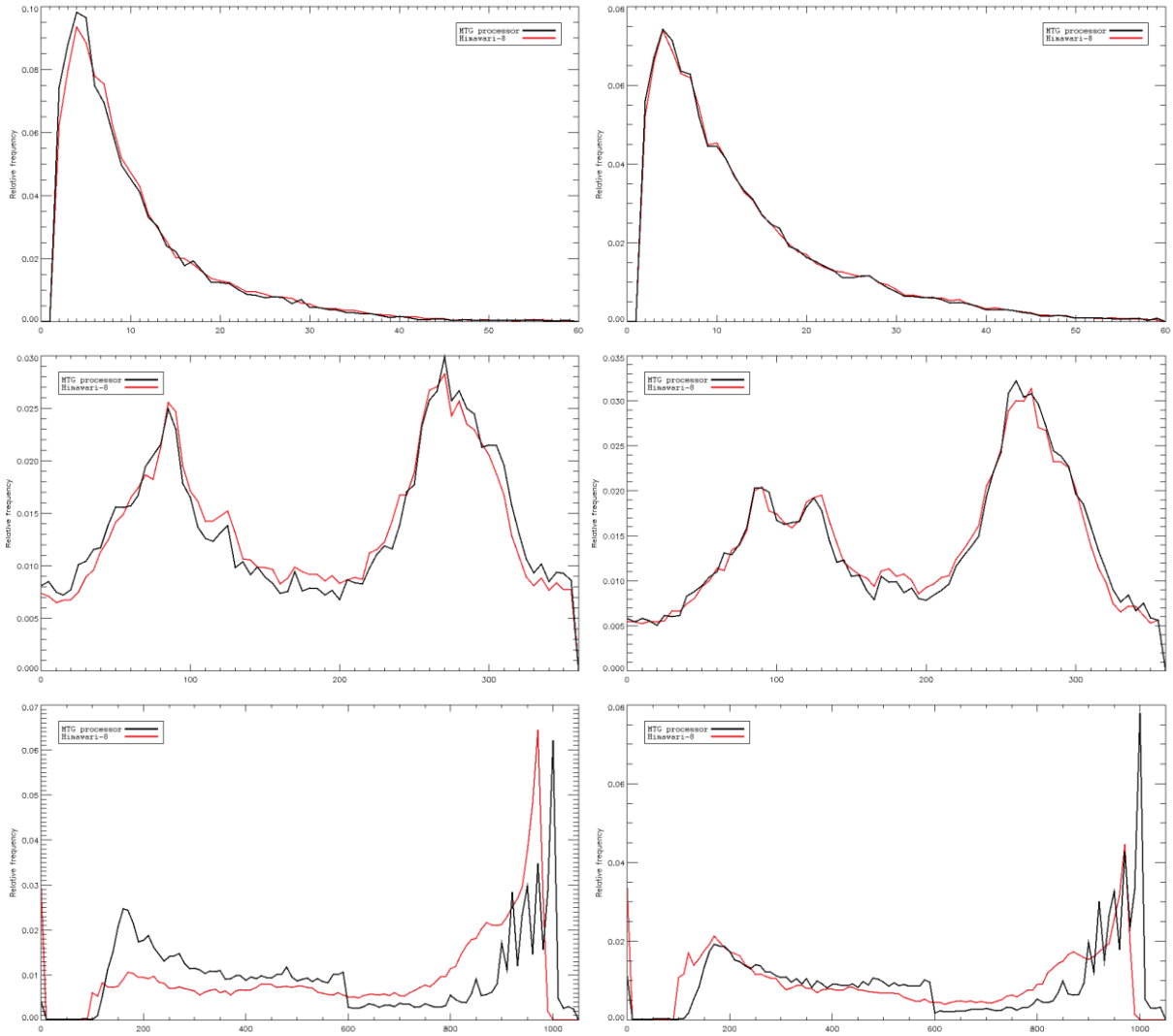

Figure 7: **Channel 0.64 µm (left) and channel 10.41 µm (right) AMV speed (top row), direction (middle row) and pressure (bottom row) histograms, for Himawari-8 (red) and the MTG processor (black).**

Figure 7 shows the channel 0.64 µm (left) and channel 10.41 µm (right) AMV speed (top row), direction (middle row) and pressure (bottom row) histograms for the considered case. The speed and direction histograms are extraordinarily similar for both channels, which indicates that the tracking is almost identical for both processors. On the other hand, the pressure histograms show the differences and features already mentioned above (e.g. higher average pressure for MTG, larger amount of very-low-level AMVs for MTG, etc.). Particularly, the peaks observed for the MTG processor at high pressure values in the pressure histograms are caused by the use of an inversion correction algorithm, which is not employed in Himawari-8, as stated above.

It is intended to process larger periods of data in the near future in collaboration with JMA and KMA, in order to obtain more meaningful conclusions. A five-day period of data has already been installed onto the development server and is ready to be processed. Additional channels (i.e. water vapour channels) will also be considered.

CONCLUSIONS

MSG nested tracking results

Nested tracking AMVs are generally found at a lower altitude than those obtained with CLA/OCA. The average AMV speed bias is in general smaller for OCA, especially in certain areas like the tropics and at low levels, then CLA and nested tracking. However, there are some issues with OCA (i.e. larger speed bias in the southern hemisphere) that require further investigations. The average speed NRMS is similar in all cases, with slightly smaller values for nested tracking.

The average AMV speed statistics (bias and NRMS) vary strongly as a function of the altitude and the geographical area. Moreover, the speed bias is very sensitive to the target box size for nested tracking, which could be an indication that there is some issue with the selection of cloud-edge pixels during the height assignment process. Currently no best nested tracking configuration has been found, although NT 20x20 seems closest to CLA than the other cases considered (NT 16x16 and NT 24x24). Further tests will be performed in the near future using a longer period of data.

A minor drawback for nested tracking is that it takes longer to compute than CLA/OCA (over twice as much). This could be an important issue to be taken into account considering its operational implementation in a near-real-time environment, where timeliness is a crucial element, but its impact is unknown as of today.

Himawari-8's AMVs

The speed and direction histograms obtained for channels 0.64 µm (VIS) and 10.41 µm (IR) are very similar for Himawari-8 and the MTG processor, giving an indication that the tracking is almost identical in both cases.

The pressure histograms are also similar, although they present a few important differences:

- the average pressure is larger for the MTG processor than for Himawari-8;
- there are more very-low-level AMVs for the MTG processor;
- there seems to be no inversion correction applied to the Himawari-8 AMVs.

All in all, the MTG AMV processor has been proved capable of processing Himawari-8 data. It is intended that the processor will be further adapted to other geostationary satellite data in the framework of the development of the MTG L2PF, which will make it a very useful tool for various purposes.

REFERENCES

Carranza, M., Borde, R. and Doutriaux-Boucher, M. (2014): "Recent changes in the derivation of geostationary atmospheric motion vectors at EUMETSAT". Proceedings of the Twelfth International Winds Workshop, Copenhagen, Denmark.

Daniels, J., Bresky, W., Wanzong, S., Bailey, A. and Velden, C. (2012): "Atmospheric motion vectors derived via a new nested tracking algorithm developed for the GOES-R Advanced Baseline Imager (ABI)". Proceedings of the Eleventh International Winds Workshop, Auckland, New Zealand.

García-Pereda, J. and Borde R. (2014): "The impact of the tracer size and the temporal gap between images in the extraction of atmospheric motion vectors". J. Atmos. Oceanic Technol., 31, 1761–1770.